On the Evolution of Porosity in Spray-Deposited Tool Steels

HAIMING HU, ZIN H. LEE, DAWN R. WHITE, and ENRIQUE J. LAVERNIA

In this article, porosity, as defined by the distribution and amount of pores in spray-deposited A-2 tool steel, was investigated. Ceramic and copper substrates were used in order to understand the influence of substrate material on the formation of porosity. Moreover, the relationship between porosity and spray distance was studied using three different spray distances together with a ceramic substrate. Distinct porosity zones were identified in the deposited material. Interstitial and gas-related porosity were both present in the deposits. Experimental results show that the optimum parameters correspond to a 178-mm deposition distance, in the case of a ceramic substrate. The experimental results suggested that the pore formation mechanism in spray-deposited materials is closely dependent on the thickness of the mushy layer in the upper surface of the deposit during the spray-forming process. The thickness of the mushy zone is determined by the solid fraction contained in the impinging droplets and the thermal-transfer conditions. Moreover, the deposition angle appears to closely influence the pore morphology, as well as the thickness of the surface porosity band of the deposits. Finally, the present results suggest that residual internal stress may be an important factor in influencing crack formation in the spray-deposited tool steel.

I. INTRODUCTION

ONE of the most important characteristics of spray-deposited materials is the presence of discontinuities or pores in the materials. Because spray-forming processing essentially involves the deposition of discrete liquid, semiliquid, and solid droplets on a deposition surface, such defects may occur during solidification as a result of one or a combination of the following mechanisms: gas entrapment, interstitial porosity, and solidification shrinkage.[1–5] Although porosity is not always deleterious in spray-deposited materials, it is generally undesirable, especially for applications where strength and ductility are critical. Porosity should be reduced to the lowest possible value by optimizing the spray-deposition conditions or by thermomechanical processing. Regardless of the significant importance of porosity on the performance of spray-deposited materials, porosity in spray-deposited materials remains a critical factor in many applications, and the underlying mechanisms remain far from being understood.

Gas-related porosity is anticipated as a result of the limited solid solubility of inert gases in most structural materials. It has been suggested that the formation of gas pores is related to the presence of an excessive proportion of liquid during deposition. For the same material, porosity is relatively high when the liquid fraction is high.[6] On the other hand, the solubility and reactivity of gases used in spray deposition may also affect the formation of gas pores. Experimental results indicate that the materials produced using Ar as an atomization gas consistently exhibit a higher amount of porosity than those produced using N_2 as the atomization gas.[7] It has been argued that nitrogen may react to form nitrides with alloying elements, thereby reducing the partial pressure of N_2 in the pores.[6–9] However, in view of the irregular morphology of pores, it is highly improbable that, in all cases, a large proportion of the porosity originates from the rejection of entrapped gases, since gas porosity generally exhibits a spherical morphology. The formation of shrinkage porosity is due to a lack of feeding liquid in the dendritic mushy zone or from a riser, such as those present during ingot casting.

Available experimental evidence suggests that a large proportion of the porosity that is observed in spray-deposited materials may be attributed to interstitial porosity. This type of porosity is generally a result of the incomplete filling of the interstices between partially solidified droplets.[1] Accordingly, these types of pores are present primarily at former droplet boundaries and exhibit a highly irregular morphology. This mechanism is closely dependent on the thermal condition that is present throughout the deposited material.

In recent years, several investigations have addressed various aspects of porosity formation in spray-deposited materials. The thermodynamic properties of the materials being spray deposited, the thermodynamic properties of the atomization gas, and the solidification conditions, as well as considerations pertaining to apparatus design, are all important to the properties of the final deposit.[3–5,10,11] Bew-Lay and Cantor[12,13] studied the porosity distribution in spray-deposited materials as a function of thickness, and proposed that there are three distinct zones of porosity for Sn-38 wt pct Pb alloy and 316L stainless steels, *i.e.*, an upper band (surface), a lower band (bottom), and a central portion. The amounts of porosity in the upper and lower bands are both relatively high. For example, the volume fraction of porosity in the lower band of commonly used alloys, such as Al-4 wt pct Cu, IN718, and low-carbon steel, is generally high, in the range from 6 to 30 pct.[7,14]

Surface porosity has been attributed to two possible sources: a decrease in the gas-to-melt flow rate ratio (GMR) and a termination of the incident droplet spray.[15] For central

HAIMING HU, Postdoctoral Associate, and ENRIQUE J. LAVERNIA, Professor, are with the Department of Chemical and Biochemical Engineering and Materials Science, University of California at Irvine, Irvine, CA 92697. ZIN H. LEE, Professor, is with the Department of Materials Science and Engineering, RASOM, KAIST, Taejon, 305-701, Korea. DAWN R. WHITE, Principal Engineering Specialist, is with the Materials Systems Reliability Department, Ford Research Laboratory, Dearborn, MI 48121.

Manuscript submitted April 20, 1999.

zone porosity, Grant and Cantor[16] studied the evolution of steady-state porosity in an Al-4 wt pct Cu alloy and reported that decreasing the gas flow rate and the deposition distance led to increases in the temperature and the fraction of liquid phase at the upper surface of the spray-deposited material. They argued that an excessive amount of liquid promotes the formation of porosity. Substrate porosity is mainly influenced by the efficient dissipation of thermal energy of the material in the vicinity of the substrate.[12,14,16–18] Annavarapu and Doherty[5] reported that when the weight fraction of liquid phase in the incident droplet spray was low (*e.g.*, $f_1 = 0.2$), there was not sufficient liquid phase in the vicinity of the substrate to fill all of the interstices.

More recently, the application of spray forming as an alternative approach to manufacturing tool steel has attracted considerable interest. The impetus for using spray-forming approaches to process tool steels is to develop a cost-effective, reliable manufacturing technique to rapidly fabricate prototype metal mold tooling. For high bend-strength, hardness, and wear-resistance applications, the porosity in tool steel should be reduced to the lowest possible value by optimizing the spray-deposition conditions or by thermal mechanical processing. So far, there has been some work pertaining to the microstructural and mechanical properties of Spray-deposited tool steels,[19,20,21] but experimental and theoretical studies on porosity-formation mechanisms are very limited. The objective of the present article was to provide insight into the mechanisms that govern the porosity formation in spray-deposited A-2 tool steel. The type, amount, and distribution of porosity in the deposits was investigated *via* the variation of deposition distance and substrate thermal conductivity, in order to optimize spray-forming conditions.

II. EXPERIMENTAL PROCEDURES

The alloy used in the present investigation was A-2 tool steel, supplied as as-rolled rods (approximately 19-mm-diameter and 914-mm-long). The spray-forming details described elsewhere.[1] An A-2 tool steel bar charge of 4000 g mass was placed in a zirconia crucible. The charge was induction melted and superheated to 1630 °C and then spray atomized, using nitrogen gas at a dynamic pressure of 2.1 MPa, and deposited onto a substrate. The substrate rotation rate was 30 rpm. The mass flow rates of the atomizing gas and melt were 65 and 49 g/s, respectively. In the present study, two types of deposition substrates were used: a copper substrate, which was water cooled and positioned at a distance of 254 mm from the atomization nozzle, and a ceramic substrate (RESCORE* 780 cer-cast ceramic), which has a square surface of 150 × 150 mm with three deposition distances, as described in Table I.

*RESCORE is a trademark of Cotronics Corporation, Brooklyn, NY.)

An Inframetrics ThermaCAM SC-1000 focal-plane array infrared radiometric thermal imaging system was used to monitor and record the real-time thermal distributions over the surface of the deposit during deposition. A photograph of the apparatus is shown in Figure 1. *In-situ* temperature measurement was conducted using a type B thermocouple to measure the temperature on the deposit surface during spray deposition. Using this temperature (1329 °C) and the simultaneous thermal image taken from the deposit surface, the emissivity of the tool steel at that temperature (1329 °C) was estimated. By adjusting the emissivity over a high-temperature range (>800 °C), the thermographs can offer information about the instant temperature distribution on the deposit surface during cooling. Moreover, the temperature history of particular points of interest can also be determined from consecutive measurements.

Table I. Processing Conditions of Spray-Deposited A-2 Tool Steel

Experiment Number	Substrate Type	Deposition Distance (mm)	Deposit Height (mm)
1	ceramic	178	67
2	ceramic	254	66
3	ceramic	330	26
4	copper	254	75

Fig. 1—Photograph of the infrared radiometric thermal imaging systems.

The geometry of the spray-deposited A-2 tool steel exhibited a contour akin to the Gaussian distribution of droplets impacting on the substrate.[22] The preforms were sectioned across the center with wire electrical discharge machining (EDM), and the porosity distribution was characterized by examining the overall macrostructure and measuring densities at some specific locations. Four representative samples from each zone—the bottom, surface, center, and periphery—were sectioned from each deposit in order to conduct a microstructural examination and density measurements. These samples, with approximate dimensions of 10 × 10 × 10 mm, were then mechanically ground. Once this procedure was conducted, the densities were measured by using Archimedes' principal according to ASTM standard B328-94. Here, the theoretical density (7.86 g/cm^{-3} for A-2 tool steel[23]) was taken to determine the percentage of porosity, on the basis of density measurements, as

$$P = (1 - \rho_e/\rho_t) \times 100 \text{ pct} \quad [1]$$

where P is the porosity, and ρ_e and ρ_t are the experimentally determined density and the theoretical density, respectively.

Microstructural examination was conducted on these density samples. The samples were etched with 3 pct nital

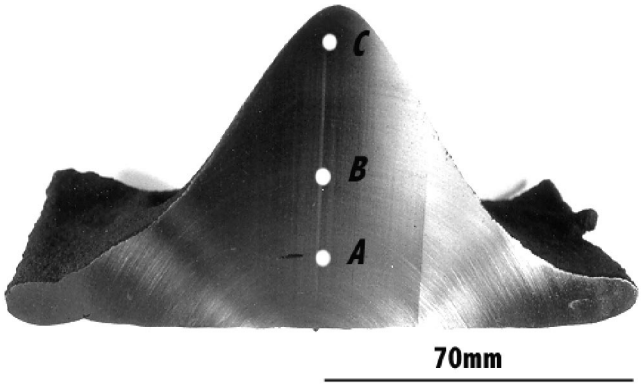

Fig. 2—Residual stress measurement positions on the surface of a half-cut deposit.

reagent. Examinations were conducted to establish the morphology of the pores present in the deposited tool steel using a Nikon Epiphot optical microscope and a Hitachi-S500 scanning electron microscope (SEM).

Residual stresses were measured using the X-ray diffraction technique (Proto Manufacturing Ltd., Ontario, Canada); one of the samples is shown in Figure 2. Both axial- and radial-direction stresses were measured in each location. The three measured locations were 15 mm (A), 35 mm (B), and 60 mm (C) above the bottom of the deposit, respectively.

III. RESULTS

A. *Distribution of Porosity*

The porosity distribution in spray-deposited tool steel can be classified, in accordance with the amount and morphology of pores, into four zones, as shown in Figure 3, (*i.e.*, a surface band, a central zone, a bottom band, and a peripheral zone, which is located on the circumference of the deposit), regardless of the deposition distance or substrate type selected. This result is consistent with the results obtained with other spray-deposited materials.[12,13] In the present study, the thickness of each zone varies with the spray distance and type of substrate, as shown in Table II. In the case of the ceramic substrate, the surface-band thickness tends to decrease and the bottom-band thickness increases with increasing deposition distance. Interestingly, when comparing experiment 2 to 4, both of which have the same deposition distance of 254 mm, the bottom-band thickness decreases with the ceramic substrate, while the surface-band thicknesses are almost the same.

Table III shows the amount of porosity at each zone under

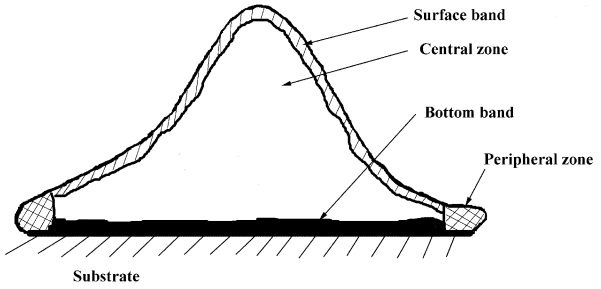

Fig. 3—Schematic of the porosity distribution in the A-2 tool steel deposit.

Table II. Thickness of Porosity Bands in A-2 Tool Steel Deposits (mm)

Experiment Number	Deposition Distance	Surface Band	Bottom Band
1	178	5.5	4.0
2	254	5.0	5.0
3	330	4.5	5.5
4	254	5.0	8.5

different processing conditions. Consistent with macrostructural observation of the half-cut surfaces of the deposits, the porosity is high in both the surface band and bottom band and relatively low in the central zone. It is noted that the surface-porosity amounts in Table III were measured from the tops of the deposits, which might be lower than those in other locations of the surface bands. The present study also shows a similar pore distribution with a spray-deposited steel preform produced using a rotating roll substrate:[14] the porosity at the peripheral region is consistently higher than that along the centerline of the preform. The results in Table III show that the deposition distance significantly affects the amount of porosity in every zone. In the center zone, for example, the porosity amount is at a minimum when the deposition distance is 178 mm, with a ceramic substrate. Increasing the deposition distance resulted in an increase of porosity. Especially with a distance of 330 mm, the porosity in the bottom band is relatively high. It is noted that the deposition distance also affects the overall yield of deposited material. The deposits are 67, 66, and 26 mm in height for experiments 1 through 3, respectively, whereas the diameters of the bottoms are almost the same. The yield of deposit 3, with a 330-mm deposition distance, is only 43 pct, whereas the other two (1 and 2) are about 70 pct. Accordingly, the present results suggest an optimum distance of 178 mm.

The dominant influence of substrate material on deposit is reflected by the porosity in the bottom band. In addition to the increased thickness of the bottom band, as shown in Table II, the amount of porosity is higher when using a copper substrate. However, there is almost no difference in the center zone and surface band of the deposit for both the copper and ceramic substrates. The porosity characteristics in each zone are discussed in the following sections.

B. *Surface-Band Porosity*

Figure 4 shows the irregular pores formed at the surface band of a deposit. The volume fraction of pores ranges from 0.93 to 4.15 pct, and the pore size is within 5 to 30 μm. It is interesting to note that the porosity varied in morphology

Table III. Distribution of Porosity in Different Positions of A-2 Tool Steel Deposits (Percent)

Experiment Number	Deposition Distance (mm)	Bottom	Center	Surface	Periphery
1	178	1.27	0.13	1.69	12.47
2	254	1.86	0.74	0.93	7.56
3	330	5.95	1.47	4.15	10.11
4	254	8.27	0.90	1.02	10.43

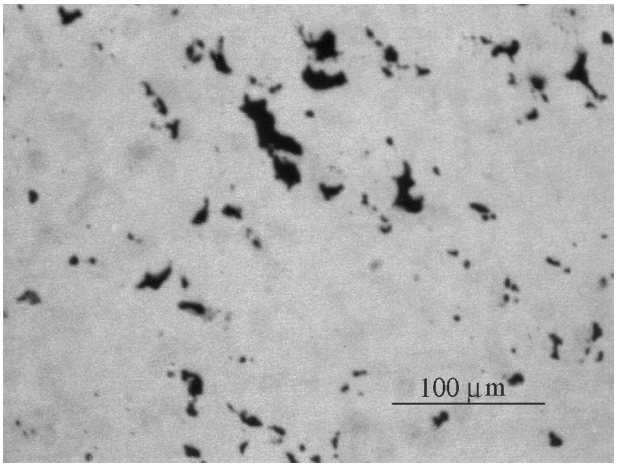

Fig. 4—Morphology of pores in surface band of the A-2 tool steel deposit.

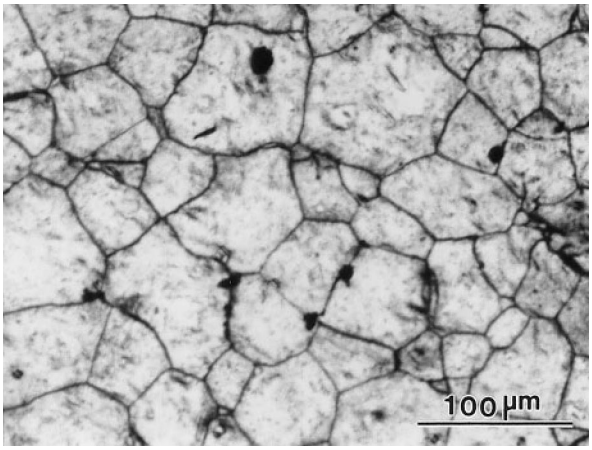

Fig. 6—Morphology of pores in center zone of the A-2 tool steel deposit.

and amount in the surface bands, as a function of location. In the vicinity of the deposit top, the porosity is relatively low. However, in a certain range away from the top zone, it was observed that the amount of porosity increased and that these pores were interconnected, forming a directional porous column. The extreme condition is illustrated in Figure 5, where pore columns are in a direction nearly parallel to the spray axis. As the distance from the top along the deposit surface increases, this phenomenon becomes less frequent.

C. *Center-Zone Porosity*

Figure 6 shows the porosity in the center zone of the deposits. The volume fraction of pores in this zone is generally minimal, ranging from 0.13 to 1.47 pct. Depending on the deposition distance and substrate material, at least more than one type of porosity was observed in this zone. In Figure 6, pores may be classified as follows. First, there are some spherical pores that are located both in the grain interiors and at the grain boundaries, in the size range of 5 to 20 μm. Second, there are irregular pores with a size less than 10 μm, present primarily at the grain boundaries. Similar observations of porosity size and distribution have been documented by a number of other investigators.[17,24–26] In accordance with the pore morphology, two types of porosity may exist in this zone: an interstitial porosity with an irregular shape at grain boundaries and gas-related porosity with a spherical shape, located at the interior of grains or at grain boundaries. It was argued in these studies that the amount and type of porosity in this steady-state zone is primarily dependent on the proportion of liquid and solid phases during deposition.

D. *Bottom-Band Porosity*

The typical porosity present at the bottom band in A-2 tool steel is shown in Figure 7. Regardless of the spray-deposition conditions used in the present study—a ceramic substrate with a 178-mm deposition distance—(Figure 7(a)) or a copper substrate with a 254-mm deposition distance (Figure 7(b)), the pore volume fraction in this band remained relatively high. The porosity amount in Figure 7(a) is much lower than that in Figure 7(b). As summarized in Table III, the amount of porosity was measured as 1.27 pct using a ceramic substrate and as 8.27 pct using a copper substrate. The variation of deposition distance and type of substrate did appear to induce some changes in porosity. For example, in Figure 7(b), small pores increased in number with an accompanying increase in the total amount of porosity in this zone. Moreover, it is noted that pores in this band have a wide size range between 0.5 and 50 μm, and they can also be classified into two types: interstitial porosity or gas-related porosity, according to the pore morphology. These two types of pores are more clearly shown in Figure 8, where interstitial pores are located at grain boundaries and gas pores are at the interiors of grains.

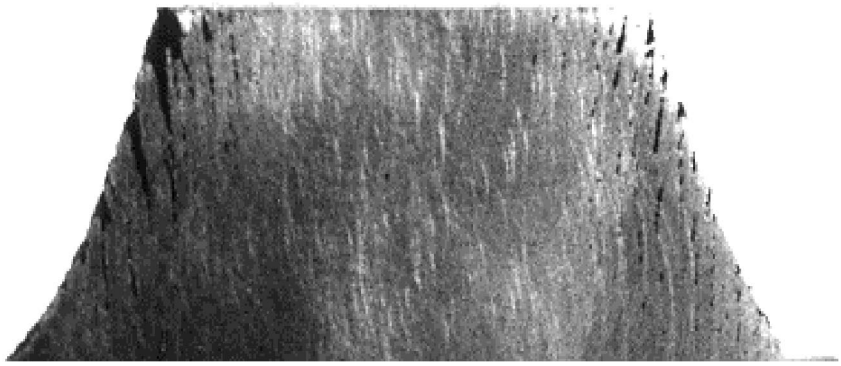

Fig. 5—Porous columns in a surface band.

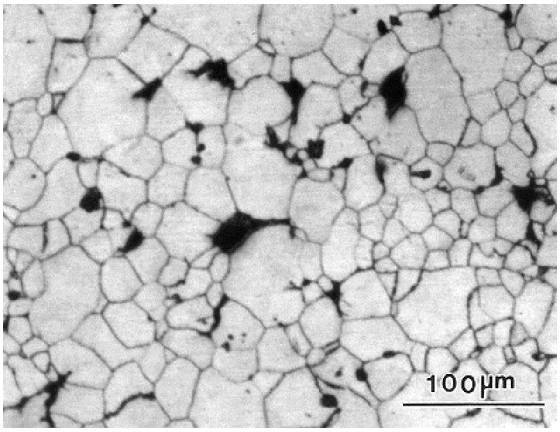

(*a*)

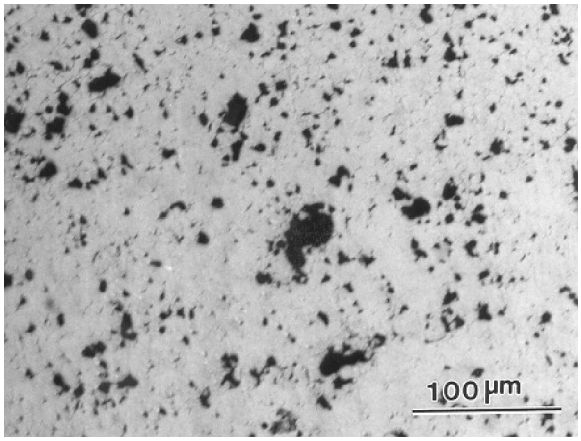

(*b*)

Fig. 7—Morphology of pores in bottom band of the A-2 tool steel deposit: (*a*) experiment 2 and (*b*) experiment 4.

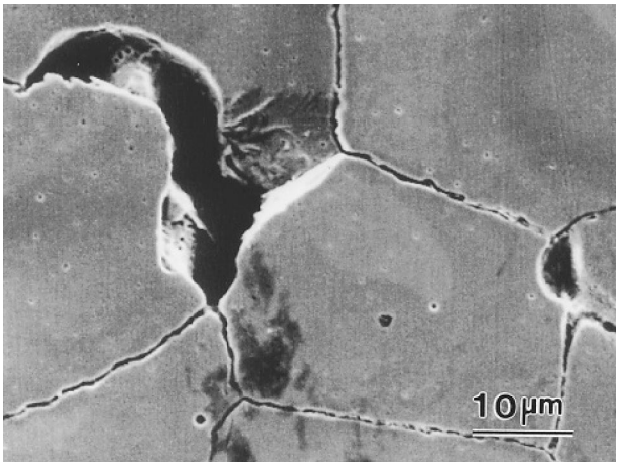

(*a*)

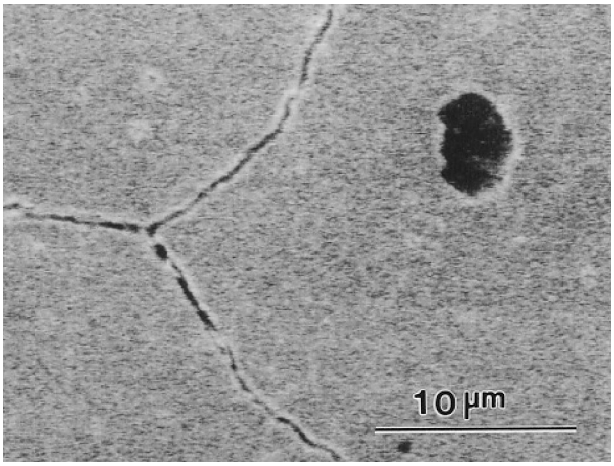

(*b*)

Fig. 8—Morphology and location of pores in A-2 tool steel deposits: (*a*) irregular transgranular pores and (*b*) gas-related pores in grain.

Macrostructural observation on the half-cut surface of the deposits revealed that there are some cracks in the 3- to 15-mm band from the substrate surface, with a length of 0.5 to 4.0 mm, as shown in Figure 9(a). The maximum crack dimension present in experiment 2 approached 8 mm, as shown in Figure 2. The orientation of these cracks was parallel to the substrate. It is noted that the number of this type of cracks is higher in the deposits using a copper substrate than in those using a ceramic substrate. From Figure 9(a), it is obvious that the deposit exhibits a layerlike macrostructure and that the cracks exist in layer boundaries. A high-magnification SEM observation of one end of a crack shows intergranular cracking characteristics, as shown in Figure 9(b), which have a tendency to propagate. Although this type of defect is not as prevalent as porosity, it is detrimental to performance, as the working conditions of tool steels require high hardness and impact resistance in the case of die applications.

E. *Peripheral-Zone Porosity*

Apart from the three regions discussed previously, the peripheral zone of the deposit may be described using the combined characteristics of the bottom and surface bands, although it has its specific characteristics with respect to porosity. The measurement results summarized in Table III reveal that the porosity at the peripheral region is always higher than that in other regions. In the peripheral zones of these spray-deposited A-2 tool steels, pore sizes are about 50 μm, with some of them perhaps reaching 1 mm in size. The microstructure in this region is layered with pores present at the boundaries of layers, as shown in Figure 10. It is worth noting that droplets may be discerned in this region, which appear to have experienced either plastic deformation or fracture. These are characteristics of a spray containing a large proportion of solid phases during impingement. Another important fact is the difference in grain size in this region with respect to the center zone. Figure 11 shows the grain morphologies in both the peripheral and center zones of deposit 3. The figures illustrate that the grain size in the peripheral region is finer and less uniform than that in the center zone. These results are consistent with the laser-diffraction measurements reported by McDonell *et al.*,[27] which reveal that the average size of droplets that are typically present at the peripheral region of a metal spray is smaller than that along the centerline of the spray cone. Moreover, it is well documented that the Gaussian droplet-size distribution that is characteristic of most metal sprays leads to a decrease in the droplet size and, hence, liquid fraction in the periphery.[28]

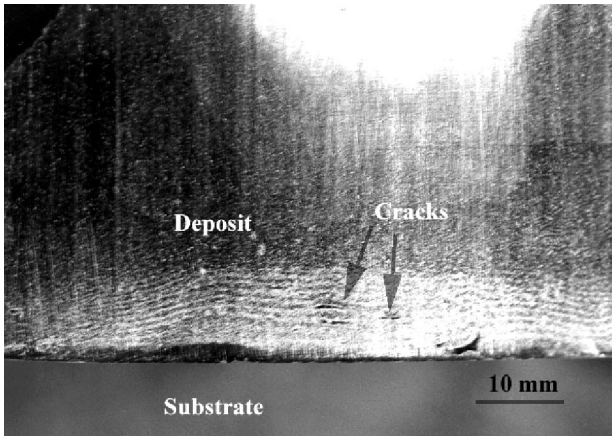

(*a*)

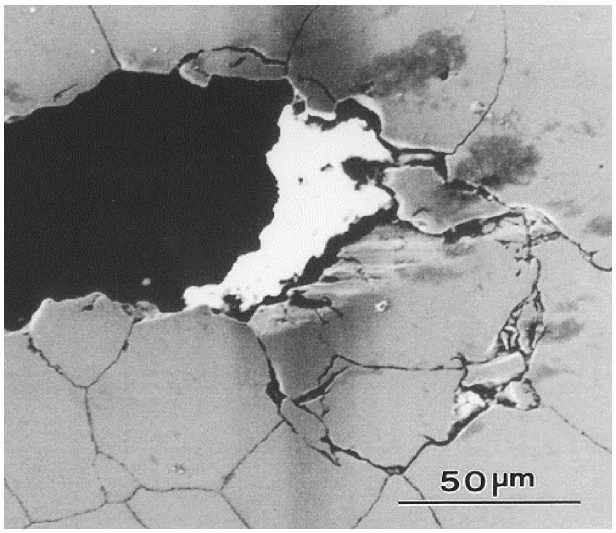

(*b*)

Fig. 9—(*a*) Macrostructure of voids in half-cut surface of a deposit and (*b*) intergranular cracking at one end of a void at high magnification.

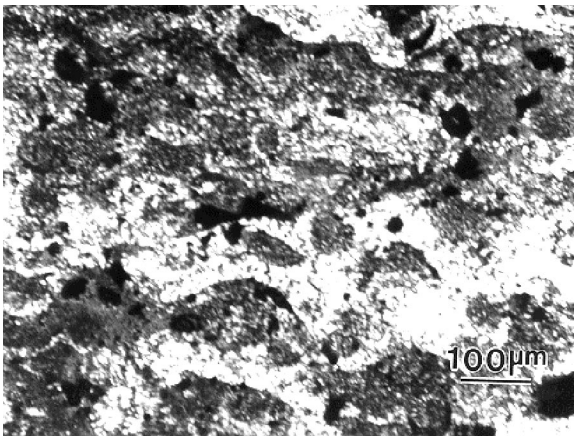

Fig. 10—Morphology of pores in peripheral zone exhibiting a layered structure.

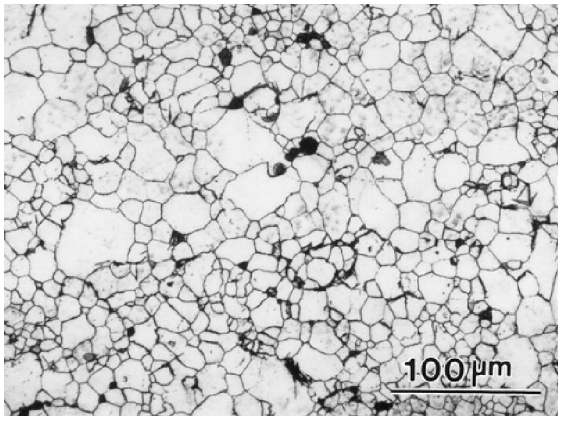

(*a*)

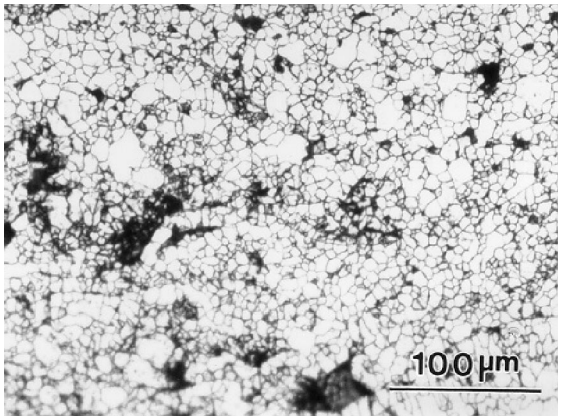

(*b*)

Fig. 11—Microstructure of spray-deposited tool steel: (*a*) center zone and (*b*) peripheral zone.

IV. DISCUSSION

Regarding the origin of porosity in spray-deposited materials, a number of trends are evident. The thermal and solidification conditions of the liquid droplets during impact will influence the mushy layer on the upper surface of the deposit. This effect will, in turn, affect the amount and morphology of pores. The relation between the mushy layer and porosity type is schematically illustrated in Figure 12. An important mechanism affecting porosity in spray-deposited materials is the formation of interstices as the metal droplets impact on one another and overlap when the mushy layer thickness is thin. In this case, the level of porosity is determined mainly by a balance between the solid/liquid ratio and the packing efficiency of the droplets. In related studies, Liu *et al.*[29] reported that the fraction of solidified particles in spray-deposition processing is a significant factor influencing the spreading behavior of droplets and the formation of micro- and macroporosity among deposits. Since these solid droplets essentially do not deform or flatten to any significant extent during impact, there is insufficient liquid to fill the interstices, leading to the creation of pores.

Gas-related porosity is also an important phenomenon in spray-deposited preforms. The gases are primarily from two sources: one is from adsorbed gases on droplet surfaces and the other stems from dissolved gas in the molten metal. Figure 13 shows the nitrogen solubility in iron in equilibrium with gaseous nitrogen at atmospheric pressure.[30] This result reveals that there is a drastic reduction in gas solubility as iron solidifies. Any dissolved gas would have a tendency to nucleate, grow, coalesce, and escape during solidification. Hence, gas pores will form as the solidification velocity

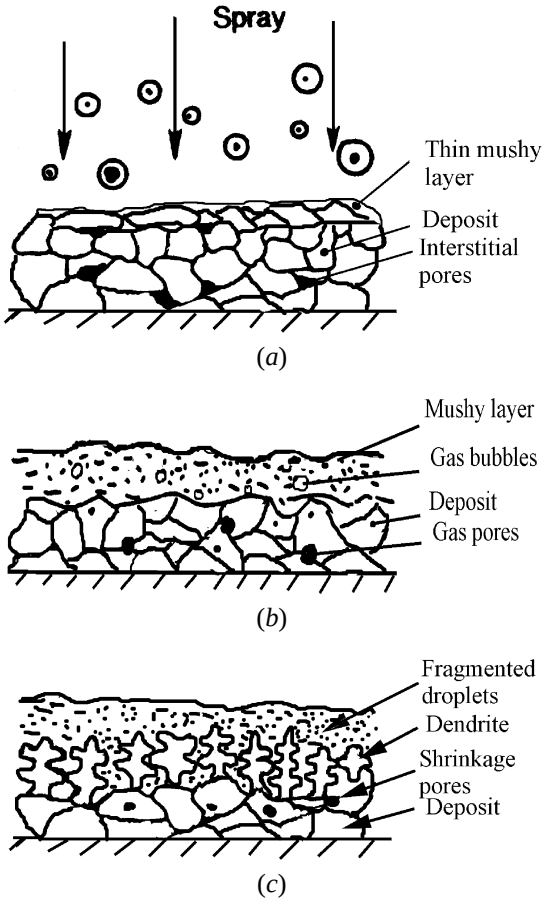

Fig. 12—Schematic of porosity formed in mushy layer: (*a*) interstitial pores, (*b*) entrapped gas pores, and (*c*) solidification shrinkage pores between dendrites.

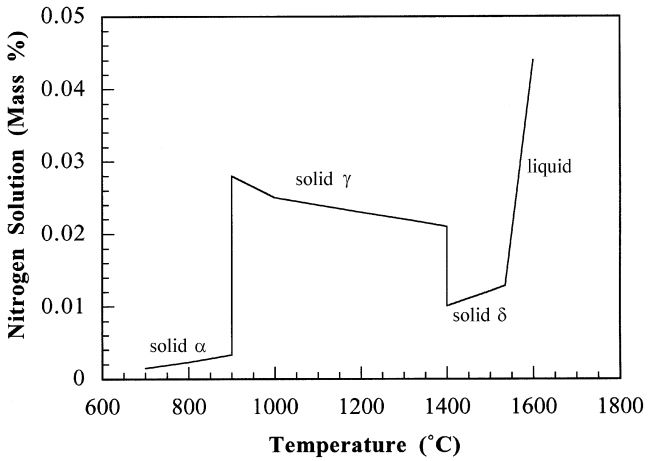

Fig. 13—Nitrogen solubility in iron in equilibrium with gaseous nitrogen at atmospheric pressure.[30]

exceeds the diffusive velocity of the gaseous element. From Figure 13, it is noted that the amount of nitrogen solution in iron is 0.044 pct at 1600 °C, which equals 2.746 vol pct of nitrogen gas in iron at atmospheric pressure. The amount of gas present in the droplets is likely to exceed that corresponding to Figure 13 as a result of rapid solidification. Therefore, gas-related porosity can be attributed to both adsorbed and dissolved gases. After the mushy layer on the upper surface reaches a certain thickness, the surface is continuously disturbed by a high-velocity gas jet, and atomized droplets and the gas may be entrapped, as shown in Figure 12(b). The lower viscosity and the higher thickness of the mushy layer will lead to entrapment of gas and its coalescence during deposition. This is consistent with the argument for a gas entrapment mechanism for large spherical pores,[31,32] because trapped gas bubbles must solidify in a mushy layer to maintain their large spherical shape and size. Within a thin mushy zone, large bubbles cannot form, and smaller bubbles may migrate a short distance to the surface prior to solidification. Gas related porosity may be present intergranularly or transgranularly, depending on the solidification conditions. Noteworthy is the fact that the solidification conditions are closely related to the thickness and location of the semiliquid or mushy layer.

Solidification shrinkage can also lead to the formation of pores, although this mechanism is significant only under rather specific deposition conditions. This effect can be explained by the state of the mushy layer on the upper surface of the deposit during spray deposition. For a spray-deposited Cu-6 wt pct Ti disk, for example, if the liquid fraction of droplets at impingement is relatively high (such as 31 pct liquid), the thickness of the mushy layer after 30 seconds of spraying is about 18 mm at the center of the disk, and the liquid fraction of the mushy layer at the top of the growing deposit is also high.[33] Solidification shrinkage porosity can be prevented if the temperature gradient in the mushy layer is high and the interdendritic feeding is possible. On the contrary, if the temperature gradient is low and the molten material solidifies in a mushy solidification mode, the liquid metal is unable to flow through the dendrite, and shrinkage pores/cavities remain following complete solidification.

A. *Mushy Layer Formation*

The liquid fraction in the spray and the thermal environment during impingement are the key factors that govern the evolution of a mushy layer. Numerical and experimental studies of the thermal environment during deposition are available.[1–3,12,29,34] At the initial stage of deposition, the thickness of the spray-deposited material is small, and the corresponding heat conduction within the thin layer may occur relatively fast. The temperatures at the upper surface and at the deposit/substrate interface rise together and remain relatively close. The heat-transfer process in the first initial droplets is often described as Newtonian, *i.e.*, the thermal gradient inside the layer is negligible. The temperature at the upper surface of the deposit increases monotonically as the thermal mass increases. As the deposit thickness becomes higher, the temperature at the interface between the deposit and substrate decreases after reaching a maximum.[34] The temperature difference between the upper surface and deposit-substrate interface increases with the thickening of the deposited material, due to an increase of the internal conduction resistance to heat flow. During the deposition process, the temperature at the upper surface continuously increases and reaches the solidus temperature at a certain thickness. Two regimes can be divided using the solidus temperature as a reference. Before the temperature reaches the solidus temperature, the preceding droplets have already

been completely solidified prior to the arrival of the following ones, and the upper surface of the deposit is in a solid state. After the temperature exceeds the solidus temperature, the preceding droplets have not fully solidified at the moment of impingement of the following ones, and the upper surface is in a mushy state. Recent modeling work on the influence of the heat-transfer coefficient at the deposit/substrate interface[34] showed that the temperature at the upper surface of the deposit is strongly dependent upon the value of the heat-transfer coefficient. For example, the temperature at the first droplet-splat's surface at the end of a time interval is 20 °C (equal to the substrate initial temperature) for a thermal-transfer coefficient (h) value of 10^6 W·m^{-2}·K^{-1} and is 537 °C for h with 3×10^3 W·m^{-2}·K^{-1}. The value of the heat-transfer coefficient also affects the position at which the mushy layer starts forming in a deposit. As the interface h value is small ($<10^4$ W·m^{-2}·K^{-1}), or the substrate is rather insulating, like a ceramic substrate, the mushy layer is formed in an early stage, as can be compared in the porosity results in Tables II and III. Conversely, when the interfacial heat-transfer coefficient is large ($>10^5$ W·m^{-2}·K^{-1}), it becomes less influential in the formation position of the mushy layer, since the internal heat conduction within the deposited material rapidly develops as a limiting factor to heat transfer instead.

The thickness of the bottom porous region reflects the conditions of the mushy layer during the initial deposition. The ending position of the bottom porous band may correspond to the beginning position of a mushy layer with a suitable thickness. Hence, in the present investigation, the position of the mushy layer in experiment 2, with a ceramic substrate, located 4 mm away from the deposit bottom, while that in experiment 4 with a copper substrate, is 8 mm. This difference may be rationalized based on the thermal behavior of the interface, which can be described by the equation

$$k_i \frac{\partial T_i}{\partial z} = h \times (T_0 - T_{\text{sub}}) \qquad [2]$$

where k_i is the thermal conductivity of the spray-deposited material, h is the heat-transfer coefficient at the interface of the deposit/substrate, T_0 is the temperature of the deposited tool steel at the interface, and T_{sub} is the temperature of the substrate at the interface. Due to the higher surface roughness and lower thermal conductivity of the ceramic substrate, the value of ($T_{\text{sub}} - T_0$) is higher than that corresponding to the copper substrate. Therefore, the high-temperature gradient corresponding to an insulating substrate promotes the formation of a mushy layer that is closer to the interface, relative to that in a conductive substrate. This argument is consistent with previous results, which suggest that the characteristics of the bottom porous band near the substrate are governed by the thermal environment present during deposition.

It should be noted that the thermal energy transfer (convection and radiation) at the upper surface of a spray-deposited preform may also influence the behavior of the mushy zone. Related work reveals that radiation heat transfer is principally affected by the properties of the atomization gas, temperature of the preform surface, and the surface emissivity.[35] The convective heat-transfer coefficient is primarily dependent on the atomization gas velocity for a given gas chemistry and the diameter of the spray-deposited preform.[36] In the present study, all the experiments were completed using the same atomization gas and almost the same diameter of deposit. Therefore, the effect of the heat-transfer process on the upper surface is not discussed specifically in this article, although different spray-deposited distances may cause different surface temperatures.

After the deposit reaches a certain critical thickness, the magnitude of h decreases and finally reaches a relatively steady state;[3,34] the formation of a mushy layer depends primarily on the solid fraction in the impinging droplets. If the solid fraction in the droplets is high, the formation time of the mushy layer increases and, hence, the thickness would be thin. By definition, the average fraction of solid in the incident spray is determined as follows:

$$\bar{f}_s = \int_0^\infty f_s(r, z)\ \delta(r)\ dr \qquad [3]$$

where $f_s(r, z)$ is the fraction of solid of a droplet of radius r at a distance z from the nozzle, and $\delta(r)$ is the probability density function of the droplet size distribution. For a log-normal distribution, $\delta(r)$ is determined by the mass median diameter (d_m) and the geometric standard deviation (σ_g). The value of d_m can be estimated using Lubanska's equation,[37]

$$d_m = KD \left(\frac{\eta_m}{\eta_g W} \left(1 + \frac{M}{G} \right) \right)^{1/2} \qquad [4]$$

where D is the diameter of the liquid stream; W is the Weber number; η_m and η_g are, respectively, the kinematic viscosity of the melt and gas; and M and G are, respectively, the melt and gas flow rate.

Evaluating the solid fraction of a droplet of radius r at a distance Z from the nozzle requires the numerical solution of the droplet equations of motion as well as its thermal history.[38] At a given distance, a droplet can be fully liquid, fully solidified, or semisolid; depending on its size, the fraction of solid increases with decreasing droplet size. Also, the average fraction of solid increases with increasing deposition distance.

In this study, the spray-deposition processing conditions, such as the GMR, superheat temperature, atomization pressure, *etc.*, were maintained relatively constant. Therefore, the average size of the droplets in these four runs remains the same, according to Eq. [4]. The variation in deposition distance, however, leads to a change in the proportion of solid phases during impingement. For experiment 1 through 3, with a ceramic substrate, the amount of porosity in the center zone of the deposit increased with increasing deposition distance. On the basis of the relationship between the mushy layer and porosity, it was suggested that there is a critical thickness of the mushy layer. After evaluating the porosity in all experiments, it was determined that the mushy-layer thickness is optimal when the deposition distance is 178 mm.

B. *Influence of Surface Geometry*

Generally, there are different effects present when droplets impinge initially on a substrate and subsequently on each other. The droplets may bounce off, alter their morphology, and adhere onto the surface, or fracture into several secondary droplets. The spatial distribution of the droplet size inherently leads to a local variation in impingement correlation along the surface of the deposit. Accordingly, with the exception of the initial layer of impinging droplets, which encounter a relatively flat surface, most of the droplets are likely

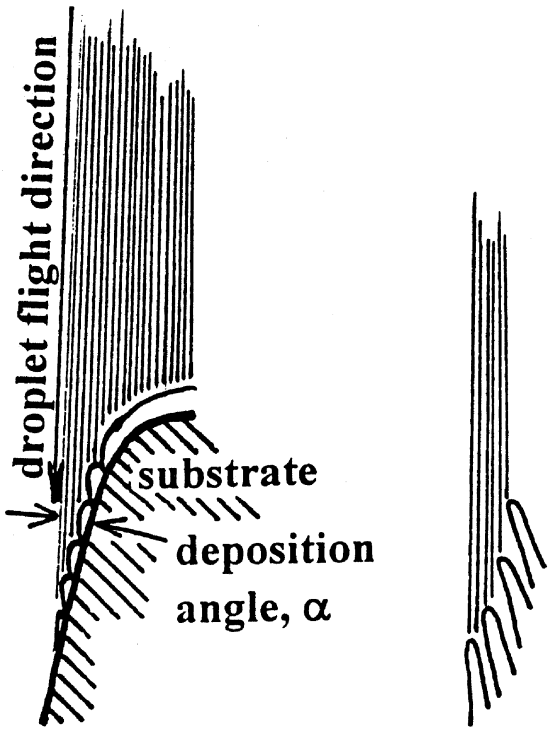

Fig. 14—Schematic formation of porous column deposition by a shadowing effect: (*a*) an initial stage and (*b*) fully developed porous column.[39]

to impinge onto an irregular surface. Liu *et al.*[29] studied the influence of surface roughness on porosity formation and argued that two processes can occur during the spreading of liquid droplets on rough surfaces. One is the separation between the deposition surface and the spreading liquid, which may eventually develop into voids if they can entrap the atomization gas or if the local heat-transfer condition in the vicinity of separation can freeze the voids. The other is the splashing of the liquid on an irregular deposition surface, which may also contribute to void formation.

In this study, a high density of irregular voids was noted in the surface bands of deposits in the form of directional porous columns; this phenomenon has been described as porous column formation (Figure 5).[39] The mechanism of porous column formation is attributed to the combined effects of shadowing and of a high solid fraction in the mushy layer on the deposit surface. The deposition angle (α) is defined as the angle between the surface tangent and the spray direction of droplet. When α decreases in magnitude, the distance between two points where neighboring droplets fall on the slanted deposit surface increases, leading to the formation of a shadow below each column, as shown schematically in Figure 14. The initial start of the porous columns can be small protrusions that form preferably on the upper edge of the slanted surface, because it is nearest to the spraying nozzle. Therefore, below the shade of the first protrusion, a subsequent protrusion will develop and the process will repeat itself.

During the final stages of spray deposition, the GMR increases, corresponding to a decrease in metallostatic pressure, and the increased solid fraction leads to the formation of interstitial porosity. If α is large, the droplets in the central region of the spray cone experience the minimum flight distance, with a correspondingly high sticking efficiency. When α decreases in magnitude, the flight distance of a droplet from the nozzle to deposit surface increases, with a corresponding increase in solid fraction. On the other hand, the number of droplets impinged on a unit of surface becomes small. Hence, on the basis of this argument, it may be deduced that interstitial porosity can form at and below a certain critical deposition angle where f_s reaches a critical value, which is reportedly 0.7 at a flight distance in the range from 300 to 400 mm.[3,4,33]

In the present study, the thickness of the surface porous band increases with increasing deposition distance, which is consistent with the previous argument. On the other hand, the shorter deposition distance usually results in a more-steep surface geometry, resulting in a smaller deposition angle at the position from the center, similar to that of the deposit with a longer deposition distance. Therefore, the feathering phenomenon is influenced not only by the deposition distance but also by the surface geometry of deposit. The porous column formation can be prevented by directing the spray axis perpendicular to the deposit surface.

C. *Influence of Residual Stress*

An interesting observation in spray-deposited A-2 tool steel is the presence of voids in the region above and near the bottom band; the voids exist along the layer boundaries. A higher proportion of the voids occurs in the deposit using a copper substrate. The voids exhibit a highly irregular morphology with intergranular cracking characteristics, as shown in Figure 9, and may be attributed to the effect of high residual stresses on the porosity formed during the initial deposition. In related studies, Knowles and King[40] measured the residual stresses induced by cold water quenching in a powder metallurgy 8090 aluminum alloy and also investigated the effect of residual stresses on the morphology of the fatigue-crack fronts. In their fatigue testing, single-edge notch-bend specimens were solution treated at 530 °C for 1 hour and quenched. They were then subject to aging treatments. The measurements revealed that surface compressive stresses are present in all the aged conditions, and that these surface compressive stresses, on the order of the yields stress, cause severe bowing of fatigue-crack fronts.

The development of residual stress in spray-deposited materials has been investigated using both experimental and numerical approaches. For example, Ho and Lavernia[41,42,43] calculated the residual stress using the finite-element method for a variety of spray-deposited materials. Assuming that a semisolid layer developed on the upper surface of the deposit during deposition, the temperature across the entire preform was assumed to increase linearly from the bottom to the top of the deposit. Accordingly, the axial stress is tensile for the upper region and compressive for the lower region of the deposited material. The radial stress is tensile for the center region and compressive for the top and bottom region.[42] In this case, the interior part of the deposit will experience a cooling rate that is slower than that present on the exterior. This is illustrated by the thermograph shown in Figure 15, which shows that the highest-temperature region was located at the interior of the spray-deposited material. As a result of this thermal gradient, a compressive residual stress will develop in the outer region of the deposit, whereas a tensile stress will be present in the inner portion of the deposit.

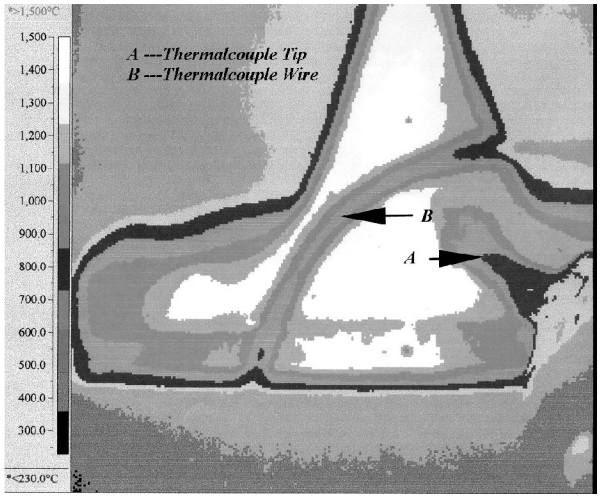

Fig. 15—Thermograph taken from the deposit surface during cooling.

Table IV. Residual Stresses Measured at Three Locations in Deposit 2 (MPa)

Stress Direction	Location A	Location B	Location C
Axial	201.2	24.2	195.0
Radial	260.4	25.5	182.6

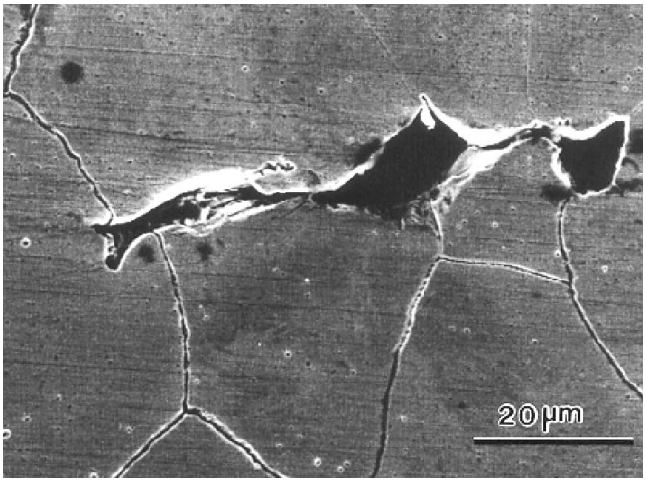

Fig. 16—Neighboring pores acting as potential void source.

In our work, residual stresses in the deposit of experiment 2, measured with an X-ray diffraction technique at three points on the half EDM-cut surface, are indicated in Table IV. The observed cracks were usually perpendicular to the spray axis, suggesting that the vertical tensile stresses play a role in their formation. It is interesting to note that the largest crack (8 mm in length) occurred at a position 15 mm above the bottom, which corresponds to the highest tensile-stress location A in the three measured locations in the deposit (Table IV). As previously noted, during the initial stage, interstitial pores readily formed at the bottom band, and most of them were located between deformed droplets. Some of them may form a large-size void directly during deposition, and some of them may form closely to each other, as shown in Figure 16. Under the effect of residual stresses, the pores propagate to form macrovoids or cracks in the deposit.

V. CONCLUSIONS

The formation of porosity in spray-deposited A-2 tool steel was investigated with different types of substrate materials and deposition distances. Based on the present study, the following conclusions can be drawn.

1. Porosity measurements show that the optimum parameters correspond to a 178 mm deposition distance, in the case of a ceramic substrate. An increase of deposition distance results in increased porosity in the deposits.
2. With respect to the copper substrate, the ceramic substrate decreases the level of porosity in the bottom band, suggesting that a substrate material with a lower thermal conductivity promotes early formation of the mushy layer.
3. The correlation of porosity and mushy-layer thickness suggests that there is an optimum mushy-layer thickness required if porosity is to be kept at a minimum value.
4. Two factors play a key role in controlling the formation of the mushy layer: the droplet solid fraction and the thermal exchange between the substrate and deposit.
5. The spray angle influences not only the sticking efficiency, but also the surface morphology of the deposits. The presence of a porous column can be prevented by maintaining the spray axis perpendicular to the deposit surface.
6. Some voids formed at the layer boundaries near the bottom porous band. With high residual stresses in the spray-deposited tool steel during cooling, some of these voids propagated and formed large cracks in the deposited materials.

ACKNOWLEDGMENTS

The authors acknowledge the financial support provided by the Ford Motor Company as well as the National Science Foundation under Grant No. CTS-9614653.

REFERENCES

1. E.J. Lavernia and Y. Wu: *Spray Atomization and Deposition*, John Wiley & Sons, New York, NY, 1996.
2. P. Mathur, D. Apelian, and A. Lawley: *Acta Metall.*, 1989, vol. 37, pp. 429-43.
3. E.J. Lavernia: *Int. J. Rapid Solidification*, 1989, vol. 5, pp. 47-85.
4. P.S. Grant, W.T. Kim, and B. Cantor: *Mater. Sci. Eng.*, 1991, vol. A134, pp. 1111-14.
5. S. Annavarapu and R. Doherty: *Int. J. Powder Metall.*, 1993, vol. 29, pp. 331-43.
6. R.H. Bricknell: *Metall. Trans. A*, 1986, vol. 17A, pp. 583-91.
7. H.C. Fiedler, T.F. Sawyer, R.W. Kopp, and A.G. Leatham: *J. Met.*, 1987, vol. 39 (8), pp. 28-33.
8. H.C. Fiedler, T.F. Sawyer, and R.W. Kopp: "Spray Forming—An Evaluation Using IN718," General Electric Report No. 86 CRD 113, General Electric, Schenectady, New York, NY, 1986.
9. M.G. Benz, T.F. Sawyer, W.T. Carter, R.J. Zabala and P.L. Dupree: *Powder Metall.*, 1994, vol. 37, pp. 213-18.
10. H. Liu, E.J. Lavernia, and R.H. Rangel: *Acta Metall. Mater.*, 1994, vol. 42, pp. 3277-89.
11. H. Liu, E.J. Lavernia, and R.H. Rangel: *J. Thermal Spray Technol.*, 1994, vol. 2, pp. 369-78.
12. B.P. Bewlay and B. Cantor: *J. Mater. Res.*, 1991, vol. 6, pp. 1433-54.

13. B.P. Bewlay and B. Cantor: in *Rapidly Solidified Materials*, P. Lee and R. Carbonara, eds., ASM INTERNATIONAL, Materials Park, OH, 1986, pp. 15-21.
14. S. Annavarapu, D. Apelian, and A. Lawley: *Metall. Trans.* A, 1988, vol. 19A, pp. 3077-86.
15. E.J. Lavernia, J. Baram, and E. Gutierrez: *Mater. Sci. Eng*., 1991, vol. A132, pp. 119-33.
16. P.S. Grant and B. Cantor: *Proc. Int. Conf. on Advanced Synthesis of Engineered Structural Materials*, J.J. Moore, E.J. Lavernia, and F.H. Froes, eds., ASM INTERNATIONAL, Materials Park, OH, 1993, pp. 263-67.
17. P.S. Grant and B. Cantor: *Cast Met.*, 1991, vol. 4, pp. 140-51.
18. M.G. Chu, D.K. Denzer, A.K. Chakrabarti, and F.R. Billman: *Mater. Sci. Eng.*, 1988, vol. A98, pp. 227-32.
19. D.N. Hanlon, W.M. Rainforth, and C.M. Sellars: *J. Mater. Sci.*, 1998, vol. 33, pp. 3233-44.
20. A.G. Leatham and R.G. Brooks: *Modern Development Powder Metall.*, 1984, vol. 15, pp. 157-73.
21. Eon-Sik Lee, Woo-Jin Park, J.Y. Jung, and S. Ahn: *Metall. Mater. Trans. A*, 1998, vol. 29A, pp. 1395-1404.
22. B.P. Bewlay and B. Cantor: *Metall. Trans. B*, 1990, vol. 21B, pp. 899-912.
23. J.R. Davis: *Tool Materials*, ASM INTERNATIONAL, Materials Park, OH, 1995, p. 135.
24. F.H. Samuel: *Metall. Trans. A*, 1986, vol. 17A, pp. 73-91.
25. E.J. Lavernia, J.D. Ayers, and T.S. Srivatsan: *Int. Mater. Rev.*, 1992, vol. 37, pp. 1-44.
26. W.D. Cai, D. Bailey, A. Sickinger, and E.J. Lavernia: *J. Thermal Spray Technol.*, 1994, vol. 3, pp. 135-41.
27. V.G. McDonell, E.J. Lavernia, and G.S. Samuelsen: in *Synthesis and Analysis in Materials Processing: Advances in Characterization and Diagnosis of Ceramic and Metal Particulate Processing*, E.J. Lavernia, H. Henein, and I. Anderson, eds., TMS, Warrendale, PA, 1989, pp. 13-37.
28. X. Liang, J.C. Earthman, and E.J. Lavernia: *Acta Metall. Mater.*, 1992, vol. 40, pp. 3003-16.
29. H. Liu, E.J. Lavernia, and R.H. Rangel: *Acta Metall. Mater.*, 1995, vol. 43, pp. 2053- 72.
30. *Smithells Metals Reference Book*, E.A. Brandes and G.B. Brook, eds., Butterworth-Heinemann Ltd., London, 1992, pp. 12-13-12-14.
31. M.G. Chu: in *Spray Forming, The Encyclopedia of Advanced Materials*, D. Bloor, R.J. Brook, M.C. Flemings, and S. Mahajan, eds., Pergamon Press, Elmsford, NY, 1994, pp. 2624-28.
32. M.G. Chu and S. John Pien: *Spray Forming Using a Linear Nozzle: Microstructure Analysis and Deposit Thermal Modeling, Proc. Julian Szekely Memorial Symp. on Materials Processing*, H.Y. Sohn, ed., TMS, Warrendale, PA, 1997, pp. 423-38.
33. P. Mathur, S. Annavarapu, D. Apelian, and A. Lawley: *Mater. Sci. Eng.*, 1991, vol. A142, pp. 261-76.
34. Q. Xu, V. Gupta, and E.J. Lavernia: *Metall. Mater. Trans. B*, 1999, vol. 30B, pp. 527-39.
35. C.G. Levi: *Metall. Trans. A*, 1988, vol. 19A, pp. 699-708.
36. J.L. Estrada and J. Duszczyk: *J. Mater. Sci.*, 1990, vol. 25, pp. 1381-91.
37. H. Lubanska: *J. Met.*, 1970, vol. 22 (2), pp. 45-49.
38. W.D. Cai and E.J. Lavernia: *Mater. Sci. Eng.*, 1997, vol. A226, pp. 8-12.
39. Z.H. Lee, H.M. Hu, D.R. White, and E.J. Lavernia: *Metall. Mater. Trans. A*, 1999, vol. 30A, pp. 1679-82.
40. D.M. Knowles and J.E. King: *Mater. Sci. Technol.*, 1991, vol. 7, pp. 1015-20.
41. S. Ho and E.J. Lavernia: *Metall. Mater. Trans. A*, 1996, vol. 27A, pp. 3241-49.
42. S. Ho and E.J. Lavernia: *Scripta Mater.*, 1997, vol. 36, pp. 283-90.
43. S. Ho and E.J. Lavernia: *Scripta Mater.*, 1996, vol. 34, pp. 1911-18.